# Experimental and simulation study on ultraviolet light emission from quaternary InAlGaN quantum wells with localized carriers

Makoto Miyoshi[a], Masataka Kato[b] and Takashi Egawa

*Research Center for Nano Device and System, Nagoya Institute of Technology, Nagoya, Aichi, 466-8555 Japan*

ABSTRACT

Different-indium-content quaternary InAlGaN multi-quantum-well (MQW) structures with the emission wavelength around 290-310 nm were grown by metalorganic chemical vapor deposition, and their emission characteristics including the indium-segregation effect were investigated by using not only experimental evaluation but also applying simulation technique, on the basis of the weakly localized exciton model.    The value of an effective localized level in the quaternary InAlGaN MQWs was estimated to be around 70 meV from the relationship between photoluminescence lifetimes and photon energies.    The simulation study, which was conducted by fitting the emission spectra, also derived the value of around 50 meV.    The present study also indicated that the quaternary InAlGaN MQW structures with the indium segregation have clear advantages over ternary AlGaN MQW ones especially in the range of dislocation density larger than approximately $1 \times 10^8/cm^2$.

a) Corresponding author;

   E-mail address: miyoshi.makoto@nitech.ac.jp (Makoto Miyoshi)

   Phone & Fax: +81-52-735-5092

b) Present affiliation: ADVICS Co. Ltd., Kariya, Aichi, 448-8688 Japan

1. Introduction

Due to their wide- and direct-transition bandgap, high-aluminum-content AlGaN systems have attracted much attention as material for light-emitting diodes (LEDs) or laser diodes (LDs) available in the mid- or deep- ultraviolet (UV) region, and for this purpose, their quantum-well (QW) structures have been researched for the past decade [1-11]. Until now, many researchers engaging in the UV light-emitting devices have focused mainly on the improvement of light-emission efficiency [1-5], because the improved efficiency would definitely put them into practical use in application fields such as sterilization, illumination and space communication. As is well known, in the group-III nitrides family, InGaN-based multi-quantum-well (MQW) structures show strong blue or near-UV light emissions despite an existence of a large number of threading dislocations (TDs) over $10^9/cm^2$. Although there has certainly been a dispute [11], this is now widely accepted as an effect of an indium segregation in the InGaN emitter layers [12-14]. According to this model, the indium segregation generates localized excitons in the bandgap and keeps the carriers from being captured at non-radiative recombination centers (NRCs) caused by kinds of crystal defects [15,16]. Thus, the non-radiative recombination rate is reduced, and the light-emission efficiency is increased as a result of the increased radiative recombination [12,16,17]. From this standpoint, AlGaN-based emitters do not have such a useful effect, different from the InGaN-based ones. Therefore, it has often been pointed out that improvement in the crystal quality of AlGaN films is indispensable for achieving high-efficiency UV-LEDs or LDs. From this prospect, many researches on AlGaN-based UV light-emitting devices have been conducted on high-quality AlN buffer films [4,18-22], or free-standing AlN substrates [23-27], which have actually shown remarkable achievements. On the other hand, the adoption of quaternary InAlGaN emitters instead of ternary AlGaN ones has also been known as another possible

solution to the realization of high-efficiency UV-LEDs [2,28].   As is the case with InGaN MQW structures, the quaternary InAlGaN MQW ones have also demonstrated superior performances, such as the internal quantum efficiency (IQE) as high as over 80% [28], probably as a result of the indium-segregation phenomenon [2,28].   Despite such a successful outcome, quantitative understanding of the localized level in the quaternary InAlGaN emitters seems to be still insufficient especially when compared to InGaN ones [12-17,29].   In order to construct the practical physical model on the quaternary InAlGaN emitters, it will be very important to achieve further information on the localized level.   In this paper, therefore, we attempted to investigate emission characteristics from the quaternary InAlGaN MQW structures.   The change in photoluminescence (PL) spectra with the incorporation of indium component was carefully investigated.   Also, a localized level in the InAlGaN MQWs was characterized by analyzing PL decay lifetimes as well as by simulating the PL spectra, on the basis of the weakly localized exciton model.

2. Experimental and simulation

Different-indium-content InAlGaN MQW structures were grown in a horizontal MOCVD system (Taiyo Nippon Sanso SR2000), where tri-methyl-gallium (TMGa), tri-methyl-aluminum (TMAl) and tri-methyl-indium (TMIn) were used as group-III sources and $NH_3$ was used as a group-V source.   A 2-in.-diameter AlN template (DOWA electronics) was employed as an underlying substrate, which has a 1-μm-thick epitaxial AlN film on a $c$-face sapphire.   The MQW structure consists of five 4-nm-thick $In_x(Al_{0.59}Ga_{0.41})_{1-x}N$ QW emitter layers separated by 7-nm-thick $Al_{0.64}Ga_{0.36}N$ barrier layers.   Prior to the growth of the MQW structure, a 1.5-μm-thick $Al_{0.66}Ga_{0.34}N$ underlying layer was grown directly on the AlN template at 1180°C without the use of any buffer

3

layers.   The threading dislocation density (TDD) of the AlGaN layer has been confirmed to be ranging from $1 \times 10^{10}$/cm$^2$ to $1.5 \times 10^{10}$/cm$^2$.   For the growth of MQW structures, the growth temperature was maintained at 850°C, and the other MOCVD parameters were also kept at constant conditions, except for the group-III input-gas ratio.    The In$_x$(Al$_{0.59}$Ga$_{0.41}$)$_{1-x}$N emitter layers with x of 0, 0.03 and 0.05 were grown under different group-III input-gas ratios in accordance with the results obtained in other experiments, where single-layer InAlGaN films were grown under various group-III input-gas ratios, and subsequently their growth rates and actual compositions were evaluated by cross-sectional scanning electron microscopy (SEM) and Rutherford backscattering (RBS) analysis, respectively.    After the MOCVD growth, surface morphology was observed by atomic force microscopy (AFM), and then, PL measurements were carried out at a room temperature (RT) and 10 K by using a 210-nm-wavelenght fourth harmonic Ti: sapphire laser as an excitation light source, where the output power was maintained at 4 mW.    PL decay lifetimes were also evaluated by using a time-resolved PL (TR-PL) measurement system, where an 80-fs-pulse-width laser with a wavelength of 210 nm was used as an excitation light source.    Time decay signals were collected by using a standard streak camera, and the minimum time resolution was approximately 15 ps. Furthermore, the simulation study was carried out using a commercially-available software SiLENSe, which has been developed especially for InGaN-based LEDs [30,31].    The simulation was performed by considering actual PL spectra, bandgap fluctuations, localized energy levels and IQEs.


3. Results and discussion

3.1. PL emission from quaternary InAlGaN MQWs

Figures 1(a), 1(b) and 1(c) show the surface AFM images for MOCVD-grown In$_x$(Al$_{0.59}$Ga$_{0.41}$)$_{1-}$

$_x$N MQW structures with x of 0, 0.03 and 0.05, respectively. As seen in these images, the surface morphologies were not markedly different between the samples regardless of the amount of indium incorporation, and all samples showed a large number of pits on their surfaces, which presumably originate from the TDs in the underlying AlGaN layer, as is often pointed out. A pit density was estimated to be approximately $1.5 \times 10^{10}$ /cm$^2$ from the AFM images for all samples, which is well consistent with the value of TDD in the underlying AlGaN layer. PL measurements were then carried out to obtain fundamental emission spectra. Figures 2(a), 2(b), and 2(c) show the typical PL spectra measured at RT and 10K for In$_x$(Al$_{0.59}$Ga$_{0.41}$)$_{1-x}$N MQW structures with x of 0, 0.03 and 0.05, respectively. Here, the peaks observed around 4.9 eV at 10K correspond to the emission from the underlying AlGaN layers. As seen in these figures, the emission from MQWs clearly shifts toward the lower energy side with the increase in the indium molar fraction, which indicates that the indium component was certainly incorporated in the emitter layers. Correspondingly, the room-temperature PL emission is obviously enhanced and broadened with the increase in the indium incorporation, where the broadening of PL emission is probably due to a bandgap fluctuation caused by the indium segregation. On the contrary, the ternary Al$_{0.59}$Ga$_{0.41}$N MQW structure showed no PL emission at RT, while a sharp PL emission peak was clearly observed at 10K. This indicates that there are many active NRCs in the AlGaN emitter layers, which were presumably caused by TDs or other crystal defects [15,16]. At the same time, it can be concluded that the indium incorporation into the emitter layers effectively reduces the non-radiative recombination rate even under the existence of such a large number of NRCs. In this study, the ratio of integrated PL intensity at RT to that at 10K was approximately treated as the experimental IQE value $\eta_{\mathrm{EXP}}$, and the resulting values of $\eta_{\mathrm{EXP}}$ are summarized in Table 1.

3.2. TR-PL study on quaternary InAlGaN MQWs

To consider the emission characteristics in more detail, TR-PL measurements were carried out. Figure 3 shows room-temperature PL decay curves for $In_x(Al_{0.59}Ga_{0.41})_{1-x}N$ MQW structures with x of 0.03 and 0.05, which were obtained around the peak emission energies. The results clearly showed that the PL lifetime was elongated with the increase in the indium incorporation. From this, it was speculated that the higher $\eta_{EXP}$ observed for the higher indium-incorporated sample is attributed to the reduction of the non-radiative recombination rate. As seen in Figure 3, semi-logarithm plots of the PL decay curves showed a non-linear shape. Therefore, the curves were fitted using a bi-exponential equation;

$$I(t) = I_1 \exp\left(-\frac{t}{\tau_1}\right) + I_2 \exp\left(-\frac{t}{\tau_2}\right) \qquad (1),$$

where $I(t)$ is the PL intensity at time $t$, and $I_i$ and $\tau_i$ represent the initial intensity and the lifetime of the $i$th component. By using this equation, PL lifetimes were derived as shown in Figure 3. In this study, we decided to treat the faster decay constant as the effective PL lifetime.

To investigate the localized level in the quaternary InAlGaN MQWs, energy dependence of PL lifetimes was analyzed. Figure 4 shows the PL spectra and the corresponding PL lifetimes at respective photon energies. The relationships between the PL lifetimes and the photon energies were fitted by using the weakly-localized exciton model [32], in the same way as ever reported for InGaN MQWs [29];

$$\tau(E) = \frac{\tau_{RAD}}{1 + \exp[(E - E_{me})/E_0]} \qquad (2),$$

where $\tau_{RAD}$ is the effective radiative lifetime, $E_{me}$ is the energy similar to the mobility edge, and $E_0$ is the effective localization depth, which represents the weakly-localized excitons into the tails of the density of states (DOS) [32]. The fitted curves are shown in Figure 4 in addition to the measured

results, and the fitting parameters are summarized in Table 1. As a result, the value of $E_0$ was estimated to be around 70 meV, as seen in Table 1, which was relatively close to the value of 60 meV reported for InGaN MQWs [29]. Thus, a localized level in the quaternary InAlGaN MQWs was experimentally obtained in the same way as the case of InGaN MQWs.

3.3. Simulation study on emission from quaternary InAlGaN MQWs

In order to investigate the emission characteristics from another point of view, the simulation study was carried out by using a software SiLENSe [30,31]. The software takes the indium-segregation effect into account by defining the bandgap fluctuation $U_{sp}$ and the effective localized levels, $U_n$ and $U_p$. $U_{sp}$ is configured to impart the shape of the emission spectra, including the dominant wavelength and the peak width [30,31]. $U_n$ and $U_p$ are localized energy levels from the conduction and valence band edges, respectively. As they assume exponential tails of DOS into the bandgap [30,31,33], $U_n + U_p$ was considered equivalent to the effective localized depth $E_0$ in equation (2). In this software, the value of $U_n + U_p$ strongly affects the calculated IQE value $\eta_{CAL}$, because all of the localized carriers are configured to contribute to the radiative recombination. The simulation was performed by fitting the calculated emission waveforms to the actual PL spectra with the use of $U_{sp}$ and $U_n + U_p$ as fitting parameters, where the comparison between $\eta_{CAL}$ and $\eta_{EXP}$ was also taken into account. Upon this simulation, the ratio of $U_n/U_p$ was kept at 7/3 in accordance with the calculated ratio of the conduction and valance band discontinuities between InN and Al$_{0.59}$Ga$_{0.41}$, which however plays almost no significant role in the simulation. Here, the bandgap energies ($E_g$) of 6.25 eV [34], 3.51 eV [34] and 0.69 eV [34], and the electron affinities of 0.6 eV [35], 1.96 eV [34] and 3.85 eV [34] were used as specific material parameters for AlN, GaN and InN, respectively, and

the band bowings for AlN-GaN, AlN-InN and GaN-InN alloys were treated as subsidiary fitting parameters. To work the software properly, a thin 10-nm-thick p-GaN layer with an acceptor density of $1 \times 10^{17}/cm^3$ was virtually inserted onto the structure, and a donor density of $1 \times 10^{16}/cm^3$ was adopted to all of the layers including MQWs. The value of TDD was kept at $1.5 \times 10^{10}/cm^2$ in accordance with the AFM observation results, which the software defines as the origin of NRCs. The power density of the excitation light was kept at 1 W/cm$^2$ in accordance with the actual PL measurements.

Figures 5(a) and 5(b) show the calculated emission waveforms for $In_x(Al_{0.59}Ga_{0.41})_{1-x}N$ MQW structures with x of 0.03 and 0.05, respectively, in which the actual PL spectra are also shown. As seen in the figures, the calculated emission waveforms are in a good agreement with the actual PL spectra. Correspondingly, the resulting values of $U_{sp}$, $U_n + U_p$, and $\eta_{CAL}$ are summarized in Table 1. From this, the value of $U_n + U_p$ was estimated to be around 50 meV, which is almost consistent with the value ever employed for simulating InGaN LEDs [30,31]. Also, it was found that there is not a large difference between the values of $U_n + U_p$ and $E_0$. Thus, a localized level in quaternary InAlGaN MQWs was estimated by the simulation study.

In addition, as a result of the simulation, the band bowing values were also derived to be 1.5 eV, 5.0 eV and 1.4 eV for AlN-GaN, AlN-InN and GaN-InN alloys, respectively, which are not significantly different from previously reported values [36-42]. Using these values, $E_g$ of quaternary $In_x(Al_{0.59}Ga_{0.41})_{1-x}N$ emitters was estimated to be 4.76 eV (260 nm), 4.55 eV (273 nm) and 4.41 eV (281 nm) for x of 0, 0.03 and 0.05 respectively, in which the figures in parenthesis are the expected wavelengths corresponding to their band-edge emission. When compared to the actual emission spectra seen in Figures 2, 4 or Figure 5, the expected wavelengths are somewhat shorter than the actual

8

dominant wavelengths, except for the ternary $Al_{0.59}Ga_{0.41}N$ alloy (x = 0).   This is probably due to an influence of the bandgap fluctuation caused by the indium segregation.   The simulation results showed that the defined bandgap fluctuation $U_{sp}$ is increased with the indium incorporation (see Table 1).   From this, the bandgap fluctuation as well as the localized level in quaternary InAlGaN MQWs was estimated by the simulation study.   Thus, the simulation technique including the physical model for InGaN LEDs seemed to be very useful even for analyzing quaternary InAlGaN MQWs.

Finally, the influence of TDD on IQE was simulated on the basis of the information above. Figures 6 shows the simulated relationships between the values of IQE ($\eta_{CAL}$) and TDD for the $In_{0.05}(Al_{0.59}Ga_{0.41})_{0.95}N$ MQW structure, which were calculated with and without a certain $U_n + U_p$ value.   From this, the IQE calculated with a certain $U_n + U_p$ value seemed to be well representing characteristics of quaternary InAlGaN MQWs; i.e., the maximum IQE as high as over 80% was reported at an emission wavelength of 282 nm for a quaternary InAlGaN MQW structure on AlGaN film with a TDD value of approximately $7.5 \times 10^8/cm^2$ [28].   On the other hand, in the case without a certain $U_n + U_p$ value, they seemed to be fairly close to experimental characteristics of ternary AlGaN MQWs rather than those of quaternary InAlGaN MQWs.   Indeed, the present $Al_{0.59}Ga_{0.41}N$ MQW structure showed a near-zero IQE at a TDD value of around $1.5 \times 10^{10}/cm^2$ as discussed in section 3.1, and other researchers also reported an IQE of approximately 60% at a wavelength of around 230-250 nm for a ternary AlGaN MQW structure with a TDD value of around $1 \times 10^8/cm^2$ [43].   The simulation results imply that IQE in AlGaN or InAlGaN MQWs without localized carriers is restricted by the existence of TDs, but that it would be considerably improved by the indium incorporation due to the formation of a localized level in the bandgap.   Thus, the present study indicated that quaternary InAlGaN MQW structures with a localized level have a clear advantage over

ternary AlGaN MQW ones, especially in the range of TDD larger than approximately $1 \times 10^8/cm^2$, which is almost consistent with the results in InGaN MQWs [30,31].

4. Summary

Different-indium-content quaternary InAlGaN MQW structures were grown by MOCVD, and their emission characteristics were investigated.  It was confirmed that room-temperature PL emission was clearly enhanced with the indium incorporation into the emitter layers.  The TR-PL measurement indicated that the increased emission was attributed to the reduction of non-radiative recombination rate.  The effective localized level caused by the indium segregation was experimentally estimated to be around 70 meV, which seemed to be close to the value reported for InGaN MQWs.  The simulation study was also carried out by fitting the calculated emission waveforms to the actual PL spectra with the use of the indium segregation model of the software.  As a result of the simulation, the effective localized level was estimated to be around 50 meV.  The present results implied that the quaternary InAlGaN MQW structures with the indium segregation have a clear advantage over ternary AlGaN MQW ones especially in the range of TDD larger than approximately $1 \times 10^8/cm^2$.  We believe that the present research method and the obtained information will contribute to the future research for nitride devices as well as to the construction of nitride-based material physics.

References

[1]   Khan M A, Shatalov M, Maruska H P, Wang H M and Kuoksts K 2005 *Jpn. J. Appl. Phys.* **44** 7191

[2]   Hirayama H 2005 *J. Appl. Phys.* **97** 091101

[3]   Shur M S and Gaska R 2008 *Proc. SPIE* **6894** 689419

[4]   Hirayama H, Yatabe T, Noguchi N and Kamata N 2010 *Electronics and Communications in Japan* **93** 24

[5]   Kneissl M, Kolbe T, Chua C, Kueller V, Lobo N, Stellmach J, Knauer A, Rodriguez H, Einfeldt S, Yang Z, Johnson N M and Weyers M 2011 *Semicond. Sci. Technol.* **26** 014036

[6]   Zhang J, Zhao H and Tansu N 2010 *Appl. Phys. Lett.* **97** 111105

[7]   Zhang J, Zhao H and Tansu N 2011 *Appl. Phys. Lett.* **98** 171111

[8]   Taniyasu Y and Kasu M 2011 *Appl. Phys. Lett.* **99** 251112

[9]   Pecora E F, Zhang W, Nikiforov A Y, Zhou L, Smith D J, Yin J, Paiella R, Negro L D and Moustakas T D 2012 *Appl. Phys. Lett.* **100** 061111

[10]  Zhang J and Tansu N 2013 IEEE Photonics Journal **5** 2600209

[11]  Smeeton T M, Kappers M J, Barnard J S, Vickers M E and Humphreys C J, 2003 *Appl. Phys. Lett.* **83** 5419

[12]  Chichibu S, Azuhata T, Sota T and Nakamura S 1996 *Appl. Phys. Lett.* **69** 4188

[13]  Narukawa Y, Kawakami Y, Funato M, Fujita S, Fujita S and S. Nakamura, 1997 *Appl. Phys. Lett.* **70** 981

[14]  Chichibu S, Wada K and Nakamura S, 1997 *Appl. Phys. Lett.* **71** 2346

[15]  Sugahara T, Sato H, Hao M, Naoi N, Kurai S, Tottori S, Yamashita K, Nishino K, Romano L T

and Sakai S 1998 *Jpn. J. Appl. Phys.* **37** L398

[16] Chichibu S F, Uedono A, Onuma T, Haskell B, Chakraborty A, Koyama T, Fini P T, Keller S, Denbaars S P, Speck J S, Mishra U K, Nakamura S, Yamaguchi S, Kamiyama S, Amano H, Akasaki I, Han J and Sota T 2006 *Nat. Mater.* **5** 810

[17] Chichibu S F, Shikanai A, Deguchi T, Setoguchi A, Nakai R, Nakanishi H, Wada K, DenBaars S P and Nakamura S 2000 *Jpn. J. Appl. Phys.* **39** 2417

[18] Chen Z, Qhalid Fareed R S, Gaevski M, Adivarahan V, Yang J W, Asif Khan, Mei J and Ponce F A, 2006 *Appl. Phys. Lett.* **89** 081905

[19] Hirayama H, Yatabe T, Ohashi T and Kamata N 2008 *Phys. Status Solidi* C **5** 2283

[20] Sakai Y, Zhu Y, Sumiya S, Miyoshi M, Tanaka M and Egawa T 2010 *Jpn. J. Appl. Phys.* **49** 022102

[21] Kim M, Fujita T, Fukahori S, Inazu T, Pernot C, Nagasawa Y, Hirano A, Ippommatsu M, Iwaya M, Takeuchi T, Kamiyama S, Yamaguchi M, Honda Y, Amano H and Akasaki I 2011 *Appl. Phys. Express* **4** 092102

[22] Mino T, Hirayama H, Takano T, Tsubaki K and Sugiyama M 2011 *Appl. Phys. Express* **4** 092104

[23] Grandusky J R, Gibb S R, Mendrick M C, Moe C, Wraback M and Schowalter L J 2011 *Appl. Phys. Express* **4** 082101.

[24] Ren Z, Sun Q, Kwon S Y, Han J, Davitt K, Song Y K, Nurmikko A V, Liu W, Smart J and Schowalter L 2007 *Phys. Status Solidi* C **4** 2482

[25] Grandusky J R, Gibb S R, Mendrick M C and Schowalter L J 2010 *Appl. Phys. Express* **3** 072103

[26] Collazo R, Mita S, Xie J, Rice A, Tweedie J, Dalmau R and Sitar Z, 2011 *Phys. Status Solidi* C **8** 2031

[27] Kinoshita T, Hironaka K, Obata T, Nagashima T, Dalmau R, Schlesser R, Moody B, Xie J, Inoue S, Kumagai Y, Koukitu A and Sitar Z 2012 *App. Phys. Express* **5** 122101

[28] Hirayama H, Fujikawa S, Noguchi N, Norimatsu J, Takano T, Tsubaki K and Kamata N 2009 *Phys. Status Solidi* A **206** 1176

[29] Chichibu S F, Marchand H, Minsky M S, Keller S, Fini P T, Ibbetson J P, Fleischer S B, Speck J S, Bowers J E, Hu E, Mishra U K and DenBaars S P 1999 *Appl. Phys. Lett.* **74** 1460

[30] Karpov S Y 2010 *Phys. Status Solidi, Rapid Res. Lett.* **4** 320

[31] Chyi E J I., Nanishi Y, Morkoç H, Piprek J and Yoon E, 2011 *Proc. of SPIE* **7939** 79391C.

[32] Gourdon C and Lavallard P 1989 *Phys. Status Solidi* B **153** 641

[33] Jacobson M A, Nelson D K, Konstantinov O V and Matveentsev A V 2005 *Semiconductors* **39** 1410

[34] Shur M, Shatalov M, Dobrinsky A and Gaska R 2012 *GaN and ZnO-based Materials and Devices, Ed. Pearton S, Springer Series in Materials Science,* **156** 83

[35] Goldberg Y 2001 *Properties of Advanced Semiconductor Materials: GaN, AlN, InN, BN, SiC, SiGe. Eds. Levinshtein M E, Rumyantsev S L, Shur M S, John Wiley & Sons, Inc.* 31

[36] Koide Y, Itoh H, Khan M R H, Hiramatu K, Sawaki N and Akasaki I 1987 *J. Appl. Phys.* **61** 4540

[37] Takeuchi T, Takeuchi H, Sota S, Sakai H, Amano H and Akasaki I, 1997 *Jpn. J. Appl. Phys.* **36** L177

[38] Onuma T, Chichibu S F, Uedono A, Sota T, Cantu P, Katona T M, Keading J F, Keller S, Mishra U K, Nakamura S and DenBaars S P 2004 *J. Appl. Phys.* **95** 2495

[39] Walukiewicz W, Li A X, Wu J, Yu K M, Ager III J W, Haller E E, Lu H, Schaff W J 2004 *J.*

*Cryst. Growth* **269** 119

[40] Onuma T, Chichibu S F, Uchinuma Y, Sota T, Yamaguchi S, Kamiyama S, Amano H and Akasaki I 2003 *J. Appl. Phys.* **94** 2449

[41] Terashima W, Che S B, Ishitani Y, Yoshikawa A, 2006 *Jpn. J. Appl. Phys*. **45** L539

[42] Davydov V Y, Klochikhin A A, Emtsev V V, Ivanov S V, Vekshin V V, Bechstedt F, Furthmüller J, Harima H, Mudryi A V, Hashimoto A, Yamamoto A, Aderhold J, Graul J and Haller E E 2002 *Phys. Status Solidi* **B 230** R4 (InN bandgap, InGaN bowing parameter)

[43] Ban K, Yamamoto J, Takeda K, Ide K, Iwaya M, Takeuchi T, Kamiyama S, Akasaki I and Amano H 2011 *Appl. Phys. Express* **4** 052101

Figure captions


Figure 1.    Surface AFM images for $In_x(Al_{0.59}Ga_{0.41})_{1-x}N$ MQW structures with x of (a) 0, (b) 0.03 and (c) 0.05.


Figure 2.    Typical PL spectra measured at RT and at 10K for $In_x(Al_{0.59}Ga_{0.41})_{1-x}N$ MQW structures with x of (a) 0, (b) 0.03 and (c) 0.05.    The peaks observed around 4.9eV at 10K correspond to the emission from underlying AlGaN layers.


Figfure 3.    Results of room-temperature TR-PL measurements for $In_{0.03}(Al_{0.59}Ga_{0.41})_{0.97}N$ and $In_{0.05}(Al_{0.59}Ga_{0.41})_{0.95}N$ MQW structures (red lines).    Blue lines represent curves by fitted using a bi-exponential equation.


Figfure 4.    Room-temperature PL spectra (red lines) and the corresponding PL lifetimes at respective photon energies (blue squares) for (a) $In_{0.03}(Al_{0.59}Ga_{0.41})_{0.97}N$ and (b) $In_{0.05}(Al_{0.59}Ga_{0.41})_{0.95}N$ MQW structures.    Blue curves represent the energy dependence of PL lifetimes fitted using the weakly-localized model.


Figure 5.    PL spectra obtained by actual PL measurements (red lines) and simulation study (blue lines), for (a) $In_{0.03}(Al_{0.59}Ga_{0.41})_{0.97}N$ and (b) $In_{0.05}(Al_{0.59}Ga_{0.41})_{0.95}N$ MQW structures, respectively.


Figure 6.    Calculated relationships between IQE and TDD for the $In_{0.05}(Al_{0.59}Ga_{0.41})_{0.95}N$ MQW structure with and without a certain $U_n + U_p$ value.

Table 1. The results of experimental IQE $\eta_{\text{EXP}}$, effective radiative lifetime $\tau_{\text{RAD}}$, energy similar to mobility edge $E_{\text{me}}$, and effective localized energy $E_0$ for InAlGaN MQW structures obtained by PL and TR-PL measurements, and calculated IQE $\eta_{\text{CAL}}$, bandgap fluctuation $U_{\text{sp}}$, and effective localized level $U_n + U_p$ derived by simulation study.

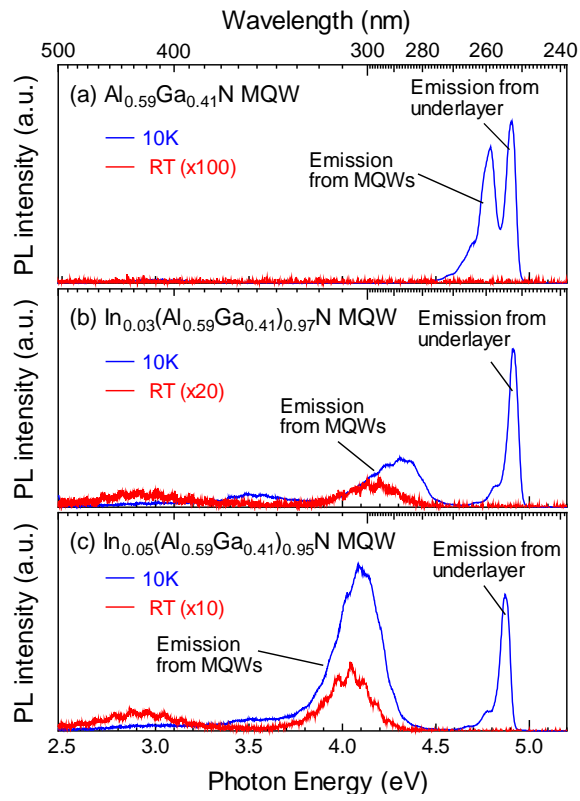| Composition in emitter layers | Results of PL and TR-PL analysis | | | | Results of simulation study | | |
|---|---|---|---|---|---|---|---|
| | $\eta_{\text{EXP}}$ (%) | $\tau_{\text{RAD}}$ (ns) | $E_{\text{me}}$ (eV) | $E_0$ (meV) | $\eta_{\text{CAL}}$ (%) | $U_{\text{sp}}$ (meV) | $U_n + U_p$ (meV) |
| $In_{0.03}(Al_{0.59}Ga_{0.41})_{0.97}N$ | 2.20 | 0.13 | 4.43 | 70 | 2.86 | 80 | 47 |
| $In_{0.05}(Al_{0.59}Ga_{0.41})_{0.95}N$ | 3.98 | 0.23 | 4.32 | 66 | 4.86 | 95 | 50 |
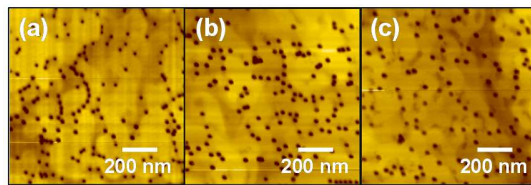
Figure 1. M. Miyoshi et al.
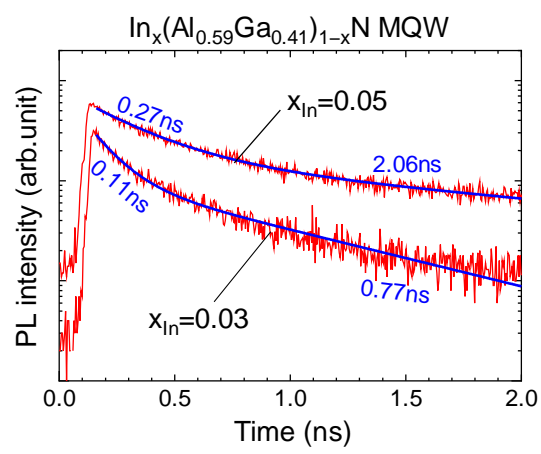
Figure 2. M. Miyoshi et al.
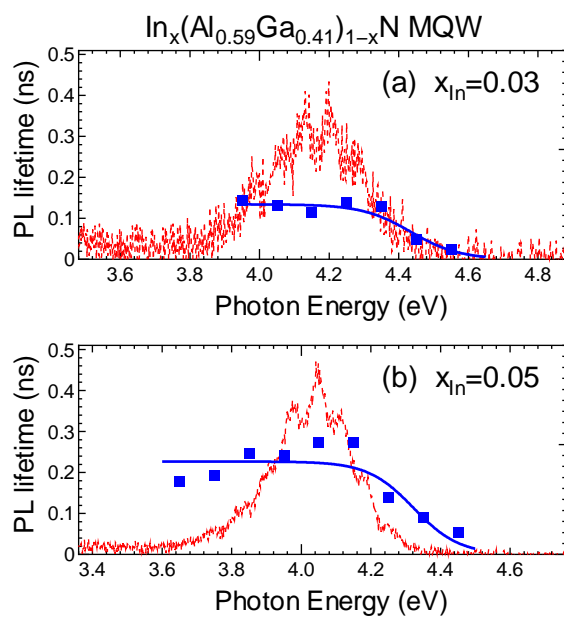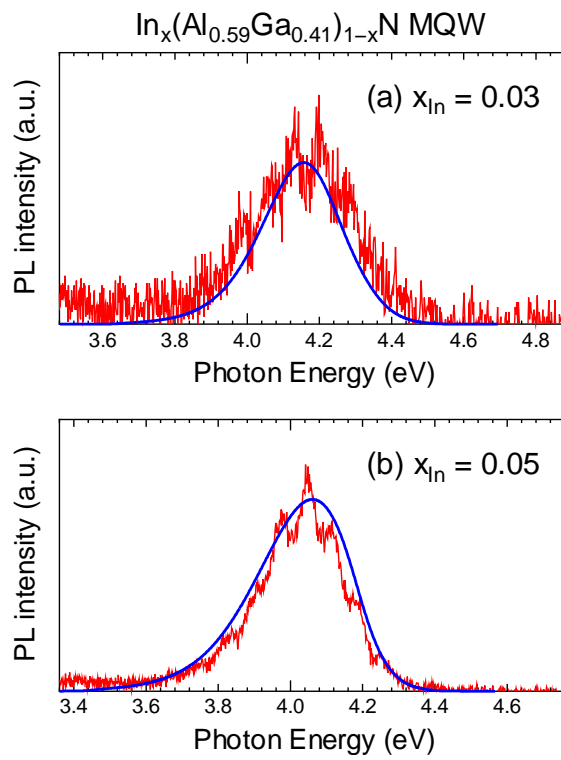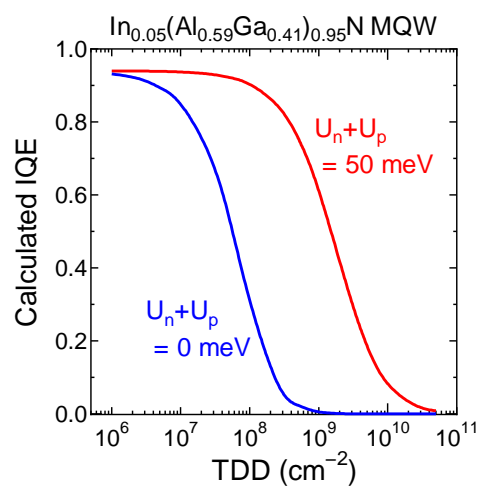
Figure 3. M. Miyoshi et al.

Figure 4. M. Miyoshi et al.

Figure 5. M. Miyoshi et al.

Figure 6. M. Miyoshi et al.